Electric conductance of a mechanically strained molecular junction from first principles: Crucial role of structural relaxation and conformation sampling

Huu Chuong Nguyen, Bartłomiej M. Szyja, and Nikos L. Doltsinis

Institute for Solid State Theory and Center for Multiscale Theory and Computation, Universität Münster, Wilhelm-Klemm-Strasse 10, 48149 Münster, Germany

(Received 28 April 2014; revised manuscript received 13 August 2014; published 29 September 2014)

Density functional theory (DFT) based molecular dynamics simulations have been performed of a 1,4-benzenedithiol molecule attached to two gold electrodes. To model the mechanical manipulation in typical break junction and atomic force microscopy experiments, the distance between two electrodes was incrementally increased up to the rupture point. For each pulling distance, the electric conductance was calculated using the DFT nonequilibrium Green's-function approach for a statistically relevant sample of configurations extracted from the simulation. With increasing mechanical strain, the formation of monoatomic gold wires is observed. The conductance decreases by three orders of magnitude as the initial twofold coordination of the thiol sulfur to the gold is reduced to a single S–Au bond at each electrode and the order in the electrodes is destroyed. Independent of the pulling distance, the conductance was found to fluctuate by at least two orders of magnitude depending on the instantaneous junction geometry.

DOI: 10.1103/PhysRevB.90.115440 PACS number(s): 71.15.Pd, 68.35.Gy, 73.63.Rt, 81.07.Pr

I. INTRODUCTION

Metal-molecule-metal nanojunctions have been studied extensively over the last decade, motivated by the quest to develop miniaturized—molecular—electronics devices. In particular, the gold–benzene-1,4-dithiolate (BDT)–gold system has been considered prototypical in this field [1–9]. Despite such intensive investigation, many points remain unsettled concerning its conductive properties. For instance, experimental conductance measurements exhibit a huge spread ranging from 10^{-4} to $0.5G_0$ (see [1,4,8,10–12] and references therein), which is partly attributed to the difficulty in controlling the precise nature of the junction geometry. For theory, on the other hand, reproducing experimental conductance data has been a major challenge, with density functional theory (DFT) based calculations often overestimating conductance by two orders of magnitude [5,13–15]. Aside from the electronic structure treatment, theoretical models often suffer from idealized junction geometries and a lack of statistics, for instance, with respect to thermal fluctuations. Most studies have represented the electrodes as a perfect Au(111) surface [5,13,16–22] and only vary the geometry of the BDT molecule or its distance to the electrode. Other works take into account the degrees of freedom of the electrode using classical molecular dynamics simulations [23–26]. However, these simulations are unable to describe accurately the different possible chemical bonding scenarios between the BDT molecule and the gold electrode. For similar reasons, the influence of mechanical strain is also poorly understood. Recently, it has been suggested that the conductance increases during elongation of a Au–BDT–Au junction [27], whereas other studies show the opposite trend [6–9]. A proper theoretical treatment requires the use of *ab initio* molecular dynamics (AIMD), due to the multiple bond breaking events that occur during the pulling of the nanojunction. Such a simulation is, however, computationally extremely demanding for realistic time and length scales.

In this work, we investigate the structural changes and their effect on the conductance of a mechanically strained Au–BDT–Au junction at finite (room) temperature using a combination of Car-Parrinello molecular dynamics (CPMD) [28] and the DFT based nonequilibrium Green's-function (NEGF) method [29]. Our aim is to obtain statistically meaningful distributions of conductance values for different pulling distances and to understand the variations in terms of the underlying evolution of the junction geometry.

II. MODEL SETUP AND COMPUTATIONAL DETAILS

Our model consists of a BDT molecule anchored on a slab of seven 4×4 Au(111) layers in a fully periodic unit cell (see Fig. 1) with fixed x and y dimensions of 11.687 and 10.213 Å, respectively, and a z length incrementally varied from 25.0 to 36.0 Å. The initially perfect top and bottom Au layers are parallel to the xy plane and are both connected to the BDT molecule through the periodic boundary conditions in the z direction (see Fig. 1). The fourth (middle) Au layer was kept fixed throughout. The CPMD simulations were carried out with the CPMD program [30] using the Perdew-Burke-Ernzerhof (PBE) functional [31,32] and Vanderbilt ultrasoft pseudopotentials [33–35] with a 25-Ry plane-wave cutoff. The time step was set to 4 a.u. (≈0.1 fs), the fictitious orbital mass was set to 400 a.u., and the temperature in the production runs was controlled by a Nosé-Hoover chain thermostat [36,37] and kept at 300 K on average. The pulling of the junction was simulated according to the following protocol. The unit cell was increased by 0.1 Å in the z direction every 5000 MD steps (≈0.5 ps). Once the box size reached a multiple of 0.5 Å, the system was left to evolve for at least 4 ps, of which the first 2 ps, at least, were found necessary to fully relax the structure, while the last 2 ps were used for further analysis. For some pulling distances, the relaxation period was significantly longer.

Conductance calculations were performed using the NEGF code TRANSIESTA [29] with the numerical double zeta basis set including polarisation functions (DZP) on a minimum of 30 snapshots taken every 2500 MD steps from the last 2 ps of trajectory at each multiple of 0.5 Å in the z direction.

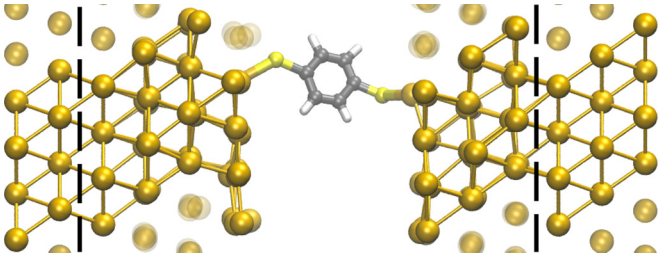

FIG. 1. (Color online) Initial simulation setup with the BDT molecule attached to two Au(111) surfaces. The dashed lines represent the CPMD unit-cell size in the z direction. The additional Au layers were added for the conductance calculations in which the scattering region included the BDT molecule and three Au layers on each side. Periodic images of Au atoms in the xy plane are shown without bonds.

III. RESULTS AND DISCUSSION

A. Pulling-induced structural changes

Let us first outline the structural changes to the junction occurring as a result of the mechanical manipulation. Figure 2 depicts snapshots from the simulation representative of the different stages of the pulling process. To illustrate the migration within the gold electrodes, the three unconstrained layers on both sides have been colored according to their initial position, the first layer red, the second layer blue, and the third layer green. At the shortest z length of $l_z = 25.5$ Å (which corresponds to a distance of 10.1 Å between the gold surfaces) all gold atoms stay in their original layers and each of the thiol S atoms is bonded to two Au atoms for most of the time. Very occasionally a short-lived third contact occurs. At $l_z = 26.0$ Å, the S atoms are starting to pull Au atoms out of the surface top layer, which allows Au atoms from the second layer to move toward the surface [Fig. 2(a)]. At 27.5 Å [Fig. 2(b)], one of the two Au–S bonds at the upper electrode has been broken and a new one has formed. Moreover, two Au atoms have been pulled out of the bottom surface, creating vacancies which are filled by Au atoms from the second layer. At 28.0 Å [Fig. 2(c)] the number of S–Au bonds is reduced to a single contact at one electrode, while there remain two S–Au bonds at the other. The top two layers of the Au slab are now significantly disordered, the Au atoms attached to the thiol groups having left the top layer and Au atoms from the second layer having migrated to the top layer. It can also be seen from Fig. 2(b) that one atom from the third layer has moved to the second layer. The next qualitative structural change takes place at 30.0 Å [Fig. 2(d)]. Both electrodes are now connected to the BDT molecule only by a single S–Au bond. As the stretching process continues, a chain of Au atoms is pulled out of the bottom electrode. When the box length reaches $l_z = 35.0$ Å, the monoatomic wire consists of three Au atoms, the one closest to the surface forming the tip of a triangle above the first Au layer [Fig. 2(e)]. A similar observation was made in a previous AIMD simulation of a related gold-thiol system [38]. Remarkably, in our simulation the second Au atom in the chain is originally from the second layer [Fig. 2(e)]. At $l_z = 36.0$ Å, the gold wire ruptures between the second and third Au atom from the BDT and the electrodes are seen to relax [Fig. 2(f)].

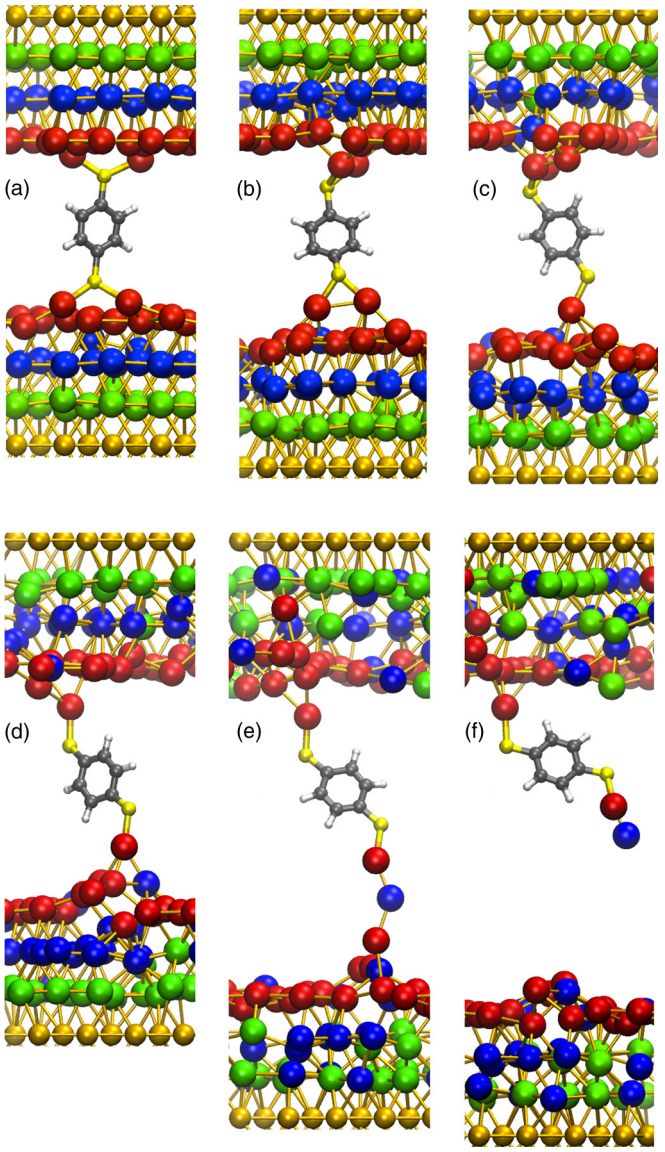

FIG. 2. (Color online) Snapshots from the simulation at different pulling stages of the Au–BDT–Au junction corresponding to the z lengths of the unit cell 26.0 Å (a), 27.5 Å (b), 28.0 Å (c), 30.0 Å (d), 35.0 Å (e), and 36.0 Å (f).

To estimate the rupture force, we have averaged the total energy at each simulated distance (Fig. 3). Assuming a Hooke-like behavior of the monoatomic wire, a quadratic function was fitted to the energy starting from a box size of 30 Å, where the monoatomic Au wire is first formed, up to bond breaking. The rupture force was determined to be 1.44 nN from the derivative of the quadratic energy function at 36.0 Å. This value is in agreement with the breaking forces of 1.4–1.5 nN obtained for a monoatomic gold chain in the literature using a variety of methods including DFT [38–40], classical MD [41], and TEM-antiferromagnetic experiments [42].

Pontes *et al.* [13] observed a rupture of the Au–S instead of the Au–Au bond, the rupture force ranging from 0.05 to 2 nN depending on the geometrical configuration before breaking. However, in these simulations the surface gold atoms were fixed at arbitrary positions, i.e., the system did not evolve naturally. A combined grand canonical Monte Carlo and

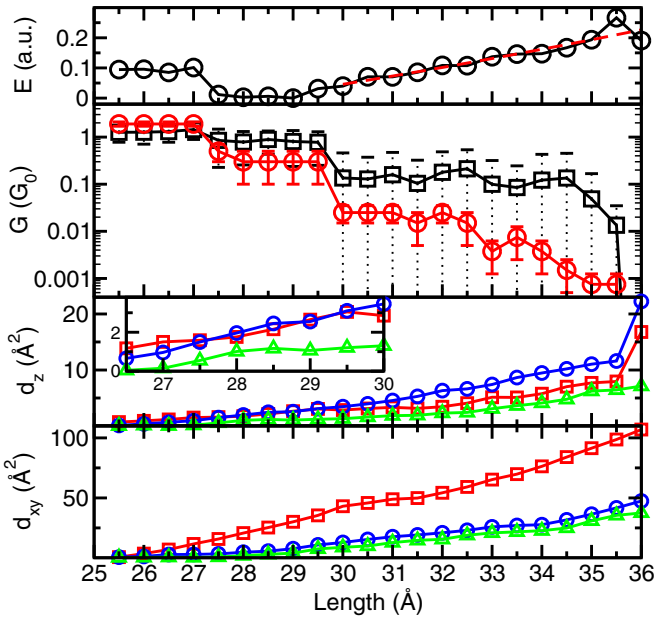

FIG. 3. (Color online) First panel: Average total energy (black solid line/circles) and quadratic regression (dashed red line). Second panel: Mean conductance with error bars corresponding to standard deviation (black line/squares) and most probable conductance value with error bars corresponding to the histogram bin size (red line/circles). Third panel: Mean-square displacement in the z direction, d_z, per Au layer (red line/squares, first layer; blue line/circles, second layer; green line/triangles, third layer). Inset: Magnified view of the regions where the steps in conductance occur. Last panel: Mean-square displacement in the xy plane, d_{xy}, per Au layer (same color scheme as above.). All quantities are plotted as a function of the unit-cell size in the z direction.

classical MD simulation of a Au–BDT–Au junction at 300 K by Pu *et al.* [43] yielded a rupture force of 0.5 nN, while they obtained a much larger value (1.5 nN) at low temperature [41]. The authors suggest that the rupture force decreases purely due to thermal fluctuations.

B. Conductance

Figure 3 shows the average conductance as a function of the box length l_z. It can be seen that the average conductance is reduced by two orders of magnitude as the system is stretched from 25.5 to 36.0 Å. Comparison of literature data on the conductance of the Au–BDT–Au junction [1,4,8,10–12] reveals variations in a similar range. A decrease in conductance with stretching distance is consistent with experimental measurements [8,11], although some recent theoretical works [25,27] predict the opposite trend. The three conductance regimes seen in Fig. 3 can be clearly linked to the junction geometry. From 25.5 to 27.0 Å, where the conductance is between 1.2 and $1.5G_0$, both BDT sulfur atoms are twofold coordinated at the Au surface [cf. Fig. 2(a)]. The first drop in the conductance down to 0.8–$0.9G_0$ at 27.5 Å occurs when one of the upper Au–S bonds is broken and another is formed during migration of the BDT on the upper surface. As discussed above, this also coincides with the onset of significant disorder in the electrodes [cf. Fig. 2(b)]. The migration of Au atoms is further illustrated by the mean-square displacement in the z direction, d_z, shown in the third panel of Fig. 3. As can be seen in the inset, the d_z curves for the first and second layer actually cross at 27.5 Å, i.e., atoms from the second Au layer begin to migrate further than Au atoms from the first layer.

For all other distances in the conductance plateau between 27.5 and 29.5 Å, the coordination of one of the S atoms is permanently reduced to a single Au–S bond while maintaining two Au–S bonds at the other electrode [cf. Fig. 2(c)]. Similarly, another drop to 0.1–$0.2G_0$ at 30.0 Å (see the second panel in Fig. 3) can be explained by the fact that both S atoms are only singly bonded to the electrode from this point onward. We conclude that the three conductance regimes are primarily determined by the number of Au–S bonds.

For each pulling distance there is a broad distribution of conductance values due to thermal fluctuations. Figure 4 shows the distribution at 30.0 Å obtained with more than 130 configurations of an extended trajectory. The distribution maximum is located in the interval [0.020, 0.025] G_0, which deviates significantly from the average of $0.12G_0$ because of rare configurations with conductance larger than $1G_0$. The corresponding results for the different pulling distances are shown in the second panel of Fig. 3, revealing changes over three orders of magnitude. For box sizes l_z between 31.5 and 33.5 Å, the calculated conductance is very close to the $0.011G_0$ reported in recent experiments [8,27]. Beyond 35.0 Å, the distribution maximum drops by another order of magnitude to below $10^{-3}G_0$.

Attempts to connect the thermal conductance fluctuations to specific vibrational modes of the junction have been inconclusive, as also described for a simpler model system elsewhere [9]. To disentangle the contributions of the molecule and the electrodes, we performed two additional simulations at $l_z = 30.0$ Å—one with frozen gold atoms and another with the BDT molecule frozen, similar to the approach used by French *et al.* [26]. The distributions for all three runs are shown in Fig. 4. It can be seen that the maxima are in the interval [0.040,0.045] G_0 for the frozen molecule and [0.045,0.050]

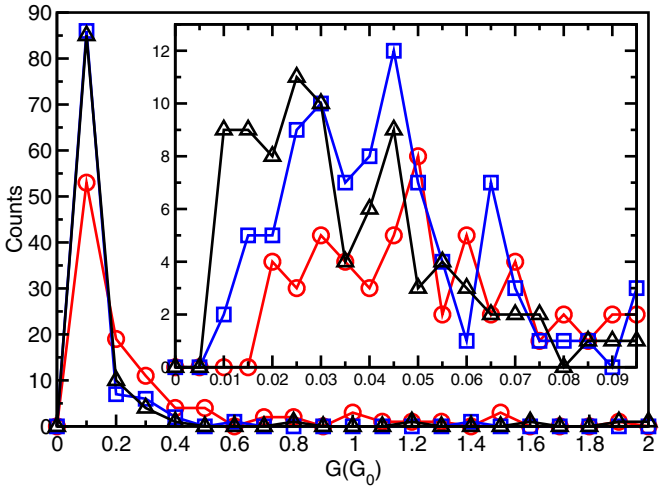

FIG. 4. (Color online) Conductance histogram of the Au–BDT–Au junction with fixed Au (red line/circles), fixed BDT (blue line/squares), and full dynamic (black line/triangles). The bin size in the inset was reduced to $0.005G_0$, while $0.1G_0$ was used for the main graph.

G_0 for the frozen electrodes, compared to [0.020, 0.025] G_0 for the unconstrained run. The comparison shows that the lowest conductance values can only be reached when the entire system is allowed to move. The largest difference from the unconstrained system is observed for the frozen electrodes, stressing the importance of a fully flexible gold surface to obtain a reliable theoretical model.

The extent of restructuring in the six unconstrained Au layers during the pulling process (the fourth, middle, layer of gold was kept frozen) is underlined by the mean-square displacements in the xy plane and in the z direction [see Figs. 3(c) and 3(d)]. Averaged over the entire simulation, i.e., all pulling stages, the computed two-dimensional diffusion coefficient in xy is 3.88×10^{-5} cm^2/s in the first layer, 1.71×10^{-5} cm^2/s in the second layer, and 1.41×10^{-5} cm^2/s in the third layer. These values are many orders of magnitude higher than the value of 10^{-40}–10^{-18} cm^2/s determined experimentally for the gold self-diffusion coefficient in thermal equilibrium at room temperature [42,44,45]. This can be explained by the fact that our simulation represents an extreme nonequilibrium situation with a pulling speed of about 20 m/s and the gold atoms being pulled out of the bulk creating vacancies and other defects (cf. Fig. 2). We have verified that this is indeed the case by performing a reference simulation of our model without mechanical manipulation, in which no diffusion was seen on the picosecond time scale.

While the mean-square displacements d_z and d_{xy} grow continuously [Figs. 3(c) and 3(d)], the conductance curve is seen to have a steplike shape. From this we conclude that the structure of the electrodes must have a minor effect on the conductance. It does, however, become noticeable for very stretched junction geometries [around 35 Å; see Fig. 3(b)], where the conductance is already low and decreases by another order of magnitude due to the disorder in the electrodes.

IV. CONCLUSIONS

To summarize, *ab initio* molecular dynamics simulations of a Au–BDT–Au junction under mechanical strain have revealed the changing coordination of the thiol sulfur atoms at the electrode surface, extensive Au restructuring of the gold electrode including the formation of a monoatomic gold wire, and the eventual rupture of a Au–Au bond. The calculated rupture force of 1.4 nN is in agreement with both theoretical and experimental data. Electronic transport calculations using the NEGF-DFT scheme along the AIMD trajectories revealed fluctuations by three orders of magnitude, highlighting the necessity of a proper statistical treatment. For stretched junction geometries with single Au–S contacts the most probable calculated conductance values agree well with experimental data, while more compressed geometries with a larger number of Au–S bonds are likely to yield conductance values that are two orders of magnitude larger than experiment. The three conductance regimes identified by us have not been discussed previously and should motivate future experimental investigations.

ACKNOWLEDGMENTS

Huu Chuong Nguyen has been partially funded by a University of Münster final year doctoral studentship. Computer time at the high-performance facility PALMA of the University of Münster is gratefully acknowledged. We thank Prof. Daniel Kosov for stimulating these simulations and for fruitful discussions.

TABLE I. Comparison of Au-Au dissociation energy (D_0) and optimal bond length (r_0).

Method	D_0 (kcal/mol)	r_0 (Å)
Experiment [46]	53.25±0.47	2.47
PBE (this work)	53.93	2.50
B3LYP [47]	45.35	2.55
CAM-B3LYP [47]	43.88	2.53
BP86 [47]	52.35	2.52
MP2 [47]	60.04	2.45
CCSD(T) [47]	47.13	2.52
LDA [48]	26.74	2.44
PW91 [48]	21.16	2.58

APPENDIX A: ACCURACY OF DFT GEOMETRIES

The accuracy of the DFT electronic structure calculations was first assessed for the Au_2 dimer. Both the equilibrium bond length and the dissociation energy agree well with experimental data and are more accurate than other theoretical data gathered from the literature (see Table I).

We have also calculated the interaction potential of a Au–S dimer with DFT using the PBE functional and coupled cluster with single, double, and perturbative triple excitations (CCSD(T)) as a benchmark (see Fig. 5). Both sets of calculations were carried out using the GAUSSIAN09 package [49] with the Stuttgart-Dresden (SDD) basis set. The PBE curve is in good agreement with the CCSD(T) reference. The relative strengths of the Au–Au and Au–S bonds are important to observe strain-induced bond rupture at the correct position within the junction.

Furthermore, we have verified that the particular DFT approach employed in our study faithfully reproduces the

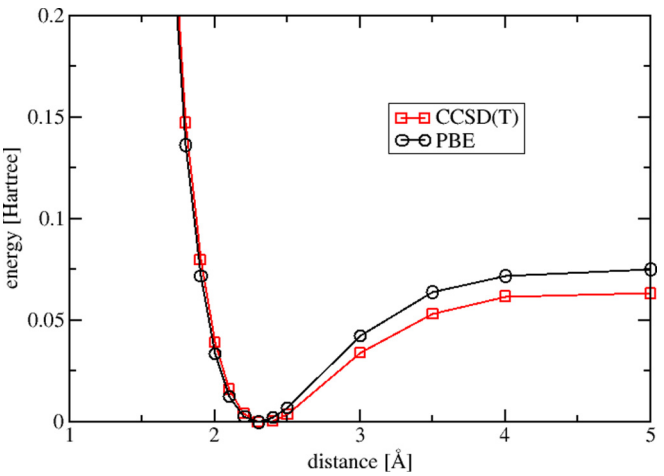

FIG. 5. (Color online) Au–S potential energy as a function of interatomic distance calculated with PBE and CCSD(T), respectively, using the SDD basis set.

TABLE II. Comparison of theoretical bond lengths and angles obtained in this work with experimental data from electron diffraction [50].

	Exp.	This work
C–C (Å)	1.39	1.40
C–S (Å)	1.77	1.77
C–H (Å)	1.09	1.09
S–H (Å)	1.35	1.35
C–C–C (°)	120.11	120.56
H–C–C (°)	119.9	119.30
C–S–H (°)	96.5	96.41

structure of the BDT molecule. The comparison in Table II between our calculated bond lengths and angles with experimental data shows very good agreement.

APPENDIX B: ACCURACY OF CONDUCTANCE CALCULATIONS

The conductance formula used for obtaining the transmission spectrum from our NEGF calculation is

$$G = G_0 T(e_F), \tag{B1}$$

where $T(e_F)$ is the transmission at the Fermi energy. It is valid only in the linear conductance regime which occurs at low voltages. Experimentally, it has been shown [1] that this regime is between -0.7 V and $+0.7$ V. Since our calculations are at zero voltage, we can safely apply the above theory. NEGF computes the steady state of a nonequilibrium system in a thermodynamical sense, as the electrodes are considered to be electron baths that can have different chemical potentials. The NEGF theory we used here is valid in the coherent transport regime, which holds for molecule sizes between 0.1 and 10 nm [51]. Since the end-to-end distance of the BDT molecule is about 0.6 nm, we are well within the allowed regime in which NEGF is valid.

TABLE III. Conductance for a single geometry at 35.0 Å with different numbers of k points.

k points	G (G_0)
$1 \times 1 \times 2$	0.0123
$3 \times 3 \times 2$	0.0182
$5 \times 5 \times 2$	0.0158
$10 \times 10 \times 2$	0.0156

Strictly speaking Eq. (B1) is only valid at low temperature; for more general cases, one should use [52]

$$G = \frac{2e^2}{h} \int T(E) \left(-\frac{\partial f_0}{\partial E} \right) dE, \tag{B2}$$

where f_0 is the Fermi function

$$f_0(E) = [1 + e^{(E-\mu_p)/k_B T}]^{-1} \tag{B3}$$

and μ_p is the chemical potential. With this formula, a convolution around the Fermi level is performed, taking into account the broadening of energy levels due to thermal fluctuations. We have checked whether Eqs. (B1) and (B2) yield significantly different results in our case. Reassuringly, the relative error in the conductance values was of the order of 10^{-2} or smaller and thus is insignificant.

Such effects would play a bigger role if there were a temperature gradient in the system, but since the entire junction was kept at the same temperature in our simulation this is not the case here.

Besides the approximations discussed above, the choice of k-point mesh can potentially have a large effect on the accuracy of the results. For all the conductance results presented in this paper, the electronic structure and transmission were computed with $1 \times 1 \times 2$ Monkhorst-Pack k-point mesh with the DZP numerical basis set and the PBE functional. The mesh cutoff was set to 200 Ry. Forty-eight Au atoms were included in each electrode; in total the system contained 204 atoms. The minimum energy for the complex integration was set to -6

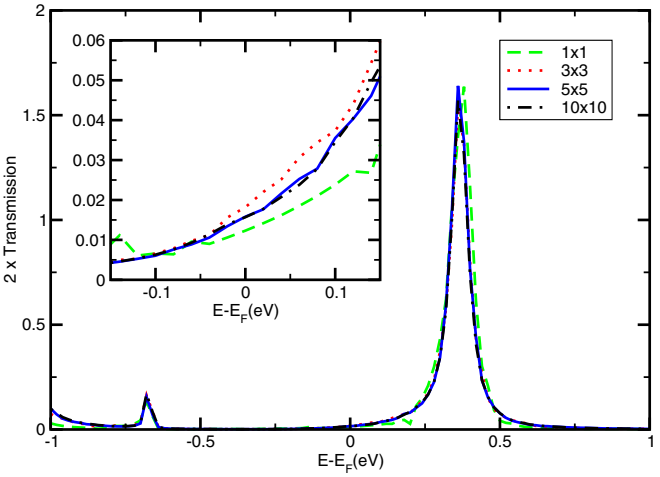

FIG. 6. (Color online) Transmission benchmark test for a single geometry at 35.0 Å with 1×1 (dashed green), 3×3 (dotted red), 5×5 (solid blue), and 10×10 k points (dotted-dashed black).

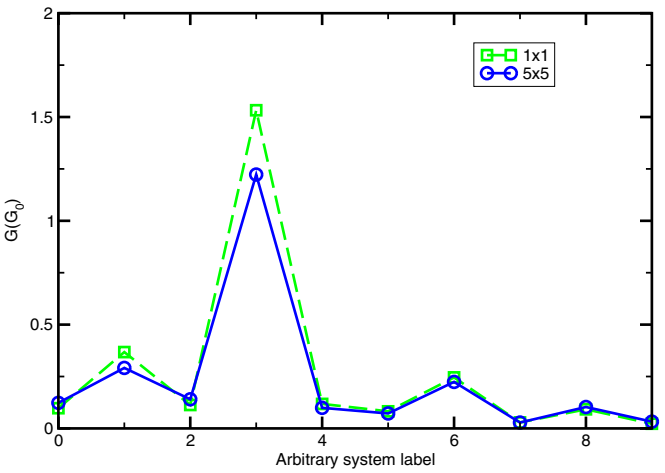

FIG. 7. (Color online) Conductance benchmark test for ten geometries taken from the CPMD trajectory at 30.0 Å ordered chronologically: 1×1 (dashed green) and 5×5 k points (solid blue).

TABLE IV. Box length in the z direction, mean conductance $\langle G \rangle$, standard deviation σ, most probable conductance G^*, and bin size used.

Length (Å)	$\langle G \rangle$ (G_0)	σ (G_0)	$G^*(G_0)$	Bin size (G_0)
25.5	1.265 95	0.489 56	1.9	0.2
26.0	1.269 70	0.562 46	1.9	0.2
26.5	1.309 43	0.531 50	1.9	0.2
27.0	1.445 00	0.555 06	1.9	0.2
27.5	0.851 00	0.624 08	0.5	0.2
28.0	0.784 65	0.528 26	0.3	0.2
28.5	0.890 40	0.457 70	0.3	0.2
29.0	0.807 24	0.569 07	0.3	0.2
29.5	0.775 09	0.523 59	0.3	0.2
30.0	0.135 52	0.325 15	0.025	0.01
30.5	0.128 88	0.245 02	0.025	0.01
31.0	0.159 05	0.313 23	0.030	0.02
31.5	0.104 17	0.219 52	0.015	0.01
32.0	0.179 14	0.307 14	0.025	0.01
32.5	0.212 41	0.325 12	0.015	0.01
33.0	0.099 79	0.218 56	0.003 75	0.0025
33.5	0.084 98	0.160 03	0.0075	0.0050
34.0	0.122 04	0.307 83	0.003 75	0.0025
34.5	0.135 25	0.317 54	0.0015	0.0010
35.0	0.048 73	0.118 58	0.000 75	0.0005
35.5	0.013 46	0.021 37	0.000 75	0.0005
36.0	0	0	0	

Ry. We have investigated the influence of k-point sampling on the transmission for a geometry taken at a z length of 35.0 Å. The results for 1×1, 3×3, 5×5, and 10×10 k points are shown in Fig. 6. Overall the 1×1 transmission is already very close to the nearly converged 10×10 transmission spectrum. In terms of conductance, 1×1 sampling yields a value of $0.0123 G_0$, deviating by only 0.003 G_0 from the 10×10 result (see Table III). Increasing the number of k points in the z direction was considered unnecessary, because the size of the system including the electrodes exceeds 46 Å.

Going beyond a single geometry, we performed another set of tests comparing the conductances calculated with 1×1 and 5×5 k points for ten geometries taken from the CPMD trajectory at 30.0 Å (see Fig. 7). We can observe that both curves follow each other closely. It is worth noting that the 1×1 results are not always below the 5×5 values, meaning that the average values are in even closer agreement. The largest deviation for any single point is 25%. Due to the high computational cost involved it would be infeasible to use 5×5 k-point sampling for all the conductance calculations in this work.

The accuracy of the DFT-NEGF approach is often assessed by comparing to results obtained with the *GW* approach, which is thought to give better results due to an improved electronic density of states. However, an exact benchmark does not exist. DFT-NEGF has been shown to yield very good agreement with experimental conductance for junctions with a hydrogen molecule or alkane chains [53].

A comparison of conductance values for a single, idealized, Au–BDT–Au configuration has been presented by Strange *et al.* [14]. Importantly, both methods give results of the same order of magnitude, the DFT value ($0.28 G_0$) being lower than the *GW* result ($0.83 G_0$). Considering that experimental results spread over four orders of magnitude [1,4,8,10–12] and conformation-dependent values fluctuate over three orders of magnitude (see this work), the DFT and *GW* results are still rather close.

APPENDIX C: STATISTICAL SAMPLING

As mentioned above and underlined by the wide spread in experimental conductance values, it is of prime importance to properly represent the junction geometry and its dynamical variations. As we show in the present paper, changes in the atomistic configuration of both the electrodes and the molecule can lead to conductance variations by three orders of magnitude. Hence proper sampling of configuration space is crucial to reproduce experiment as conductance measurements take approximately 1 ms [54], thus averaging over a large number of configurations. Our approach to calculate conductance distributions from CPMD simulations best emulates experiment. Our statistical mean values allow a much more meaningful comparison with experiment than single-point calculations on idealized geometries.

Table IV lists the mean and most probable conductance values obtained in this work for the different pulling distances together with the standard deviation and the bin size used for the histograms (see Fig. 4 for an example). These values were used for the graphs shown in Fig. 3 (second panel).

[1] M. A. Reed, C. Zhou, C. J. Muller, T. P. Burgin, and J. M. Tour, Science **278**, 252 (1997).

[2] M. Dorogi, J. Gomez, R. Osifchin, R. P. Andres, and R. Reifenberger, Phys. Rev. B **52**, 9071 (1995).

[3] R. P. Andres, T. Bein, M. Dorogi, S. Feng, J. I. Henderson, C. P. Kubiak, W. Mahoney, R. G. Osifchin, and R. Reifenberger, Science **272**, 1323 (1996).

[4] A. Nitzan and M. A. Ratner, Science **300**, 1384 (2003).

[5] J. Tomfohr and O. F. Sankey, J. Chem. Phys. **120**, 1542 (2004).

[6] B. Q. Xu, X. Y. Xiao, and N. J. Tao, J. Am. Chem. Soc. **125**, 16164 (2003).

[7] X. Y. Xiao, B. Q. Xu, and N. J. Tao, Nano Lett. **4**, 267 (2004).

[8] Y. Kim, T. Pietsch, A. Erbe, W. Belzig, and E. Scheer, Nano Lett. **11**, 3734 (2011).

[9] B. M. Szyja, H. C. Nguyen, D. Kosov, and N. L. Doltsinis, J. Mol. Model. **19**, 4173 (2013).

[10] W. Haiss, C. Wang, I. Grace, A. S. Batsanov, D. J. Schiffrin, S. J. Higgins, M. R. Bryce, C. J. Lambert, and R. J. Nichols, Nat. Mater. **5**, 995 (2006).

[11] L. Venkataraman, J. E. Klare, I. W. Tam, C. Nuckolls, M. S. Hybertsen, and M. L. Steigerwald, Nano Lett. **6**, 458 (2006).

[12] H. Hakkinen, Nat. Chem. **4**, 443 (2012).

[13] R. B. Pontes, A. R. Rocha, S. Sanvito, A. Fazzio, and A. J. R. da Silva, ACS Nano **5**, 795 (2011).

[14] M. Strange, C. Rostgaard, H. Häkkinen, and K. S. Thygesen, Phys. Rev. B **83**, 115108 (2011).
[15] M. Strange and K. S. Thygesen, Beilstein J. Nanotechnol. **2**, 746 (2011).
[16] T. Seideman, J. Phys.: Condens. Matter **15**, R521 (2003).
[17] F. Zahid, M. Paulsson, E. Polizzi, a. W. Ghosh, L. Siddiqui, and S. Datta, J. Chem. Phys. **123**, 64707 (2005).
[18] Y. Xue and M. A. Ratner, Int. J. Quant. Chem. **102**, 911 (2005).
[19] K. Hirose and N. Kobayashi, Physica E **40**, 237 (2007).
[20] K. Hirose and N. Kobayashi, Surf. Sci. **601**, 4113 (2007).
[21] W. Y. Kim and K. S. Kim, J. Comput. Chem. **29**, 1073 (2008).
[22] J. Koga, Y. Tsuji, and K. Yoshizawa, J. Phys. Chem. C **116**, 20607 (2012).
[23] M. Strange, O. Lopez-Acevedo, and H. Hakkinen, J. Phys. Chem. Lett. **1**, 1528 (2010).
[24] W. R. French, C. R. Iacovella, and P. T. Cummings, ACS Nano **6**, 2779 (2012).
[25] W. R. French, C. R. Iacovella, I. Rungger, A. M. Souza, S. Sanvito, and P. T. Cummings, Nanoscale **5**, 3654 (2013).
[26] W. R. French, C. R. Iacovella, I. Rungger, A. M. Souza, S. Sanvito, and P. T. Cummings, J. Phys. Chem. Lett. **4**, 887 (2013).
[27] C. Bruot, J. Hihath, and N. Tao, Nat. Nanotechnol. **7**, 35 (2012).
[28] R. Car and M. Parrinello, Phys. Rev. Lett. **55**, 2471 (1985).
[29] M. Brandbyge, J.-L. Mozos, P. Ordejón, J. Taylor, and K. Stokbro, Phys. Rev. B **65**, 165401 (2002).
[30] J. Hutter *et al.*, Car-Parrinello Molecular Dynamics: An *Ab Initio* Electronic Structure and Molecular Dynamics Program; see http://www.cpmd.org
[31] J. P. Perdew, K. Burke, and M. Ernzerhof, Phys. Rev. Lett. **77**, 3865 (1996).
[32] J. P. Perdew, K. Burke, and M. Ernzerhof, Phys. Rev. Lett. **78**, 1396 (1997).
[33] D. Vanderbilt, Phys. Rev. B **41**, 7892 (1990).
[34] K. Laasonen, R. Car, C. Lee, and D. Vanderbilt, Phys. Rev. B **43**, 6796 (1991).
[35] K. Laasonen, A. Pasquarello, R. Car, C. Lee, and D. Vanderbilt, Phys. Rev. B **47**, 10142 (1993).
[36] S. Nosé, J. Chem. Phys. **81**, 511 (1984).
[37] W. G. Hoover, Phys. Rev. A **31**, 1695 (1985).
[38] D. Krüger, H. Fuchs, R. Rousseau, D. Marx, and M. Parrinello, Phys. Rev. Lett. **89**, 186402 (2002).
[39] D. Krüger, R. Rousseau, H. Fuchs, and D. Marx, Angew. Chem. Int. Ed. **42**, 2251 (2003).
[40] F. Tavazza, L. E. Levine, and A. M. Chaka, J. Appl. Phys. **106**, 043522 (2009).
[41] Q. Pu, Y. Leng, L. Tsetseris, H. S. Park, S. T. Pantelides, and P. T. Cummings, J. Chem. Phys. **126**, 144707 (2007).
[42] R. Bennewitz, F. Hausen, and N. N. Gosvami, J. Mater. Res. **28**, 1279 (2013).
[43] Q. Pu, Y. Leng, X. Zhao, and P. T. Cummings, J. Phys. Chem. C **114**, 10365 (2010).
[44] R. C. Jaklevic and L. Elie, Phys. Rev. Lett. **60**, 120 (1988).
[45] D. A. Sommerfeld, R. T. Cambron, and T. P. Beebe, J. Phys. Chem. **94**, 8926 (1990).
[46] J. Ho, K. M. Ervin, and W. C. Lineberger, J. Chem. Phys. **93**, 6987 (1990).
[47] A. H. Pakiari and Z. Jamshidi, J. Phys. Chem. A **114**, 9212 (2010).
[48] E. Zarechnaya, N. Skorodumova, S. Simak, B. Johansson, and E. Isaev, Comput. Mater. Sci. **43**, 522 (2008).
[49] M. J. Frisch *et al.*, GAUSSIAN09, Revision D.01, Gaussian, Inc., Pittsburgh, 2009.
[50] G. Portalone, A. Domenicano, G. Schultz, and I. Hargittai, THEOCHEM **186**, 185 (1989).
[51] S. Datta, *Quantum Transport: Atom to Transistor* (Cambridge University Press, Cambridge, UK, 2005).
[52] S. Datta, *Electronic Transport in Mesoscopic Systems*, Cambridge Studies in Semiconductor Physics and Microelectronic Engineering (Cambridge University Press, Cambridge, UK, 1997).
[53] W. Sheng, Z. Y. Li, Z. Y. Ning, Z. H. Zhang, Z. Q. Yang, and H. Guo, J. Chem. Phys. **131**, 244712 (2009).
[54] G. Schitter and M. J. Rost, Materials Today **11**, 40 (2008).